


ARTICLE

<https://doi.org/10.1038/s41467-018-08052-6>

OPEN

Ab initio predictions for polarized deuterium-tritium thermonuclear fusion

Guillaume Hupin^{1,2,3}, Sofia Quaglioni³  & Petr Navrátil⁴

The fusion of deuterium (D) with tritium (T) is the most promising of the reactions that could power thermonuclear reactors of the future. It may lead to even more efficient energy generation if obtained in a polarized state, that is with the spin of the reactants aligned. Here, we report first-principles predictions of the polarized DT fusion using nuclear forces from effective field theory. By employing the ab initio no-core shell model with continuum reaction method to solve the quantum mechanical five-nucleon problem, we accurately determine the enhanced fusion rate and angular distribution of the emitted neutron and ^4He . Our calculations demonstrate in detail the small contribution of anisotropies, placing on a firmer footing the understanding of the rate of DT fusion in a polarized plasma. In the future, analogous calculations could be used to obtain accurate values for other, more uncertain thermonuclear reaction data critical to nuclear science applications.

¹Institut de Physique Nucléaire, IN2P3/CNRS, Université Paris-Sud, Université Paris-Saclay, 91406 Orsay Cedex, France. ²CEA, DAM, DIF, 91297 Arpajon, France. ³Lawrence Livermore National Laboratory, P.O. Box 808, L-414, Livermore, CA 94551, USA. ⁴TRIUMF, Vancouver, BC V6T2A3, Canada. Correspondence and requests for materials should be addressed to G.H. (email: hupin@ipno.in2p3.fr)

Thermonuclear reaction rates of light nuclei are critical to nuclear science applications ranging from the modeling of big-bang nucleosynthesis and the early phases of stellar burning to the exploration of nuclear fusion as a terrestrial source of energy. The low-energy regime (tens to hundreds of keV) typical of nucleosynthesis and fusion plasmas is challenging to probe due to low counting rates and the screening effect of electrons, which in a laboratory are bound to the reacting nuclei. A predictive understanding of thermonuclear reactions is therefore needed alongside experiments to achieve the accuracy and/or provide part of the nuclear data required by these applications. A salient example is the fusion of deuterium (D) with tritium (^3H or T) to generate a ^4He nucleus (α -particle), a neutron, and 17.6 MeV of energy released in the form of kinetic energy of the products. This reaction, used at facilities such as ITER¹ and NIF² in the pursuit of sustained fusion energy production, is characterized by a pronounced resonance at the center-of-mass (c.m.) energy of 65 keV above the free D and T nuclei due to the formation of the $J^\pi = 3/2^+$ resonance of the unbound ^5He nucleus. Fifty years ago, it was estimated³ that, in the ideal scenario in which the spins of the reactants are perfectly aligned in a total-spin 3/2 configuration and assuming that the reaction is isotropic, one could achieve an enhancement of the cross section by a factor of $\delta = 1.5$, thus improving the economics of fusion energy generation⁴. However, while the unpolarized cross section and some analyzing-power data exist, no correlation coefficients have been measured yet to confirm this prediction⁵. More generally, what little is known about the properties of the polarized DT fusion was inferred from measurements of the D^3He reaction⁶.

The DT fusion is a primary example of a thermonuclear reaction in which the conversion of two lighter elements to a heavier one occurs through the transfer of a nucleon from the projectile (D) to the target (T). Despite the fairly small number of nucleons involved in this process, arriving at a comprehensive understanding—in terms of the laws of quantum mechanics and the underlying theory of the strong force (quantum chromodynamics)—of the interweaving of nuclear shell structure and reaction dynamics giving rise to the DT fusion already represents a formidable challenge for nuclear theory.

Towards this goal, a pioneering ab initio study of the DT fusion was carried out in ref. 7, using a nucleon-nucleon (NN) interaction that accurately describes two-nucleon data and representing the wave function on a basis of continuous “microscopic-cluster” states⁸ made of $\text{D}+\text{T}$ and $\text{n}+^4\text{He}$ pairs in relative motion with respect to each other. However, this approach was unable to yield results of adequate fidelity, due to the omission of the three-nucleon (3N) force—disregarded for technical reasons. Numerous studies have shown that this component of the nuclear interaction is essential for the reproduction of single-particle properties^{8–12}, masses^{13–15}, and spin properties^{10,16}, all impactful in the present case. Besides the 3N force, the approach of ref. 7 also lacked a complete treatment of short-range five-nucleon correlations, which are crucial to arrive at the accurate description of the $3/2^+$ resonance. The formation of this rather long-lived resonance as a correlated, localized system of five nucleons built up during the fusion process is integral to the reaction mechanism. Finally, no polarization observables were calculated in the study of ref. 7.

In the following, we report on ab initio predictions for the polarized DT fusion using validated NN and 3N forces derived in the framework of chiral effective field theory (EFT)^{17,18}, a powerful tool that enables the organization of the interactions among protons and neutrons in a systematically improvable expansion linked to the fundamental theory of quantum chromodynamics. The quantum-mechanical five-nucleon problem is solved using the no-core shell model with continuum (NCSMC)^{10,19}, where

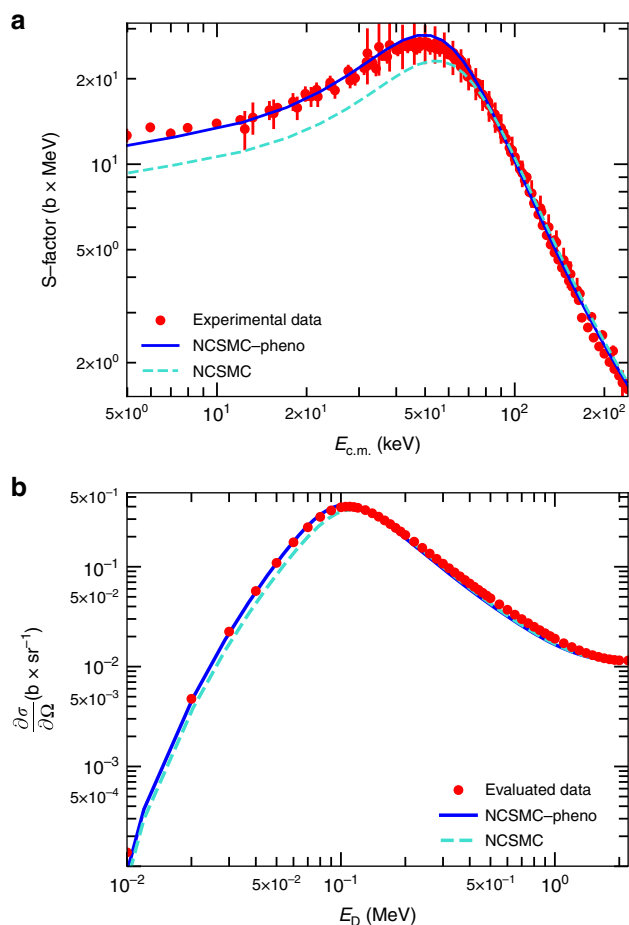


Fig. 1 Unpolarized DT cross sections. **a** Astrophysical S-factor as a function of the energy in the center-of-mass (c.m.) frame, $E_{c.m.}$, compared to available experimental data^{21–25} (with error bars indicating the associated statistical uncertainties). **b** Angular differential cross section ($\frac{d^2\sigma}{d\Omega}$) as a function of the deuterium incident energy, E_D , at the c.m. scattering angle of $\theta_{c.m.} = 0^\circ$ compared to the evaluated data of ref. 26. In the figures “NCSMC” and “NCSMC-pheno” stand for the results of the present calculations before and after a phenomenological correction of -5 keV to the position of the $3/2^+$ resonance

the model space includes $\text{D}+\text{T}$ and $\text{n}+^4\text{He}$ microscopic-cluster states, plus conventional static solutions for the aggregate ^5He system²⁰. This enables a fully integrated description of the reaction in the incoming (outgoing) channel, where the reactants (products) are far apart, as well as when all five nucleons are close together. We show that this approach yields an accurate reproduction of the DT cross section for unpolarized reactants, discriminating among reaction rates from phenomenological evaluations and demonstrating in detail the small contribution of anisotropies in the vicinity of the $3/2^+$ resonance. The maximum enhancement of the polarized cross section varies as a function of the deuterium incident energy, dropping significantly above 0.8 MeV. However, such variation is slow in the narrow range of optimal energies for the reaction, resulting in a rather constant enhancement of the rate of fusion, compatible with the historic approximate estimate.

Results

Validation of model for unpolarized reaction observables. We begin our study with a validation of our ab initio reaction method on existing experimental data for the unpolarized DT

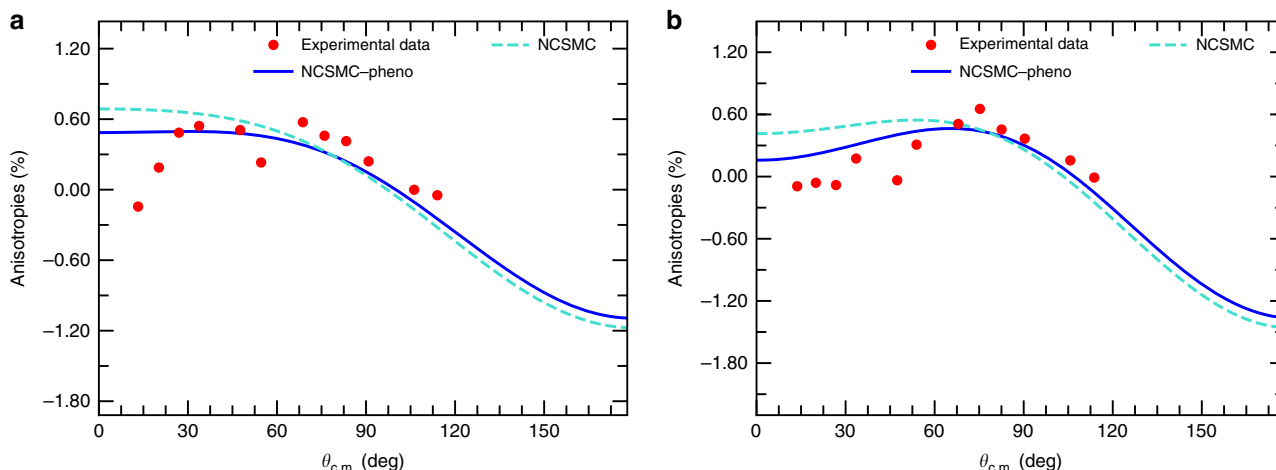


Fig. 2 Anisotropy in the unpolarized DT differential cross section. Computed and measured³⁰ percentage of anisotropies in the unpolarized angular distribution (obtained as percentage deviations from unity of the differential cross section divided by the total—angle integrated—cross section) as a function of the scattering angle in the center-of-mass (c.m.) frame, $\theta_{c.m.}$, for two values of the deuteron incident energy, E_D . **a** $E_D = 132.8$ keV. **b** $E_D = 174.7$ keV. In the figures “NCSMC” and “NCSMC-pheno” stand for the results of the present calculations before and after a phenomenological correction of -5 keV to the position of the $3/2^+$ resonance and “Experimental data” are the measurements from ref. ³⁰

reaction^{21–25}. In Fig. 1a, we review the agreement of our computed astrophysical S-factor with established measurements. The S-factor isolates the nuclear dynamics by factoring out the Coulomb component of the total reaction cross section. The experimental peak at the c.m. energy of $E_{c.m.} = 49.7$ keV corresponds to the enhancement from the $3/2^+$ resonance of ^5He (see Supplementary Note 2). We underpredict by 15% the experiment (green dashed line versus red circles), an outcome that can be traced back to the overestimation of the $3/2^+$ resonance centroid by a few keV, stemming from residual inaccuracies of the nuclear interaction¹⁰. To overcome this issue and arrive at an accurate evaluation of polarized DT reaction observables, we apply a phenomenological correction of -5 keV to the position of the resonance centroid, achieving a remarkable agreement with the experimental S-factor over a wide range of energies (blue line). A detailed explanation of how such correction was obtained can be found in the Methods section. As a further validation of our calculations in Fig. 1b we present the differential cross section in the center-of-mass frame at the scattering angle of $\theta_{c.m.} = 0^\circ$ over a range of energies up to the deuterium breakup threshold. Our results (blue solid and green dashed lines) match the differential cross section of ref. ²⁶ (red circles), obtained from a Legendre coefficient fit of measurements.

Polarization enhancement and reaction anisotropy. Having validated our calculation on precision measurements of unpolarized DT fusion, we now turn to the fusion of polarized DT fuel. The tritium has a spin of $1/2$, consequently its initial spin state is fully characterized by the Cartesian spin projection onto the axis of quantization (z -axis), q_z . On the other hand, the deuterium is a spin-1 particle. Therefore, besides the equivalent p_z projection, an extra tensor value (p_{zz}) is required to fully specify the spin state of the D beam. For the special case considered here, in which both reactants are aligned along the z -axis, the polarized differential cross section assumes a fairly simple form and is given by

$$\frac{\partial \sigma_{\text{pol}}}{\partial \Omega_{c.m.}}(\theta_{c.m.}) = \frac{\partial \sigma_{\text{unpol}}}{\partial \Omega_{c.m.}}(\theta_{c.m.}) \left(1 + \frac{1}{2} p_{zz} A_{zz}^{(b)}(\theta_{c.m.}) + \frac{3}{2} p_z q_z C_{z,z}(\theta_{c.m.}) \right),$$

where $A_{zz}^{(b)}$ and $C_{z,z}$ are the beam tensor analyzing power and spin correlation coefficient, respectively. The general expression for arbitrary orientation of the spins is more complicated and can be

found in refs. ^{27–29}. The main assumption used to estimate the 50% enhancement of the cross section for polarized DT fuel is that the reaction proceeds entirely through the $J^\pi = 3/2^+$ partial wave with an orbital relative angular momentum of the D+T pair $\ell = 0$ (that is, in an s -wave of relative motion). Under such an assumption, the unpolarized differential cross section is isotropic (that is, independent from the scattering angle). Furthermore, the integrals of $A_{zz}^{(b)}$ and $C_{z,z}$ over the scattering angle can be computed analytically and are 0 and $1/3$, respectively. This yields the estimate for the polarized reaction cross section $\sigma_{\text{pol}} \approx \sigma_{\text{unpol}} (1 + \frac{1}{2} p_z q_z)$, that is an enhancement factor of $\delta = 1.5$ when $p_z = q_z = 1$.

The study of the anisotropy in the unpolarized differential cross section stands as a first stringent test of this estimate. When investigating the angular differential cross section divided by the reaction cross section (its integral over the scattering angle), as done before in ref. ³⁰, these appear as deviations from unity. As shown in Fig. 2, a departure from a pure s -wave behavior is apparent. In particular, p -waves ($\ell = 1$) are responsible for the oblique slope, and d -waves ($\ell = 2$) for the making of a bump at 90° . Overall, we find good agreement with experiment once the centroid of the $3/2^+$ resonance is correctly located. It is worth noting that the degree of anisotropy does not exceed the 1.6% level, leading to an absolute variation of the differential cross section of about 6.6 mb between 0° and 180° . The overall good reproduction of the data gives once again evidence of the high-quality of the computed collision matrix. Thereafter we present our ab initio results including the phenomenological adjustment of the $3/2^+$ resonance centroid, and comment when appropriate, on its effect.

Validation of model for polarized reaction observables. As a further test, we computed $A_{zz}^{(b)}$ and $C_{z,z}$ from the components of the S-matrix using the formalism of the density matrix. As benchmark, we verified that (under the condition of an unpolarized target) we could reproduce the beam analyzing powers derived and computed independently. In principle both these observables can be measured in a laboratory by analyzing the differences with respect to the unpolarized cross section when the deuteron beam is vector- and tensor-polarized, the tritium is vector-polarized, and beam and target polarizations

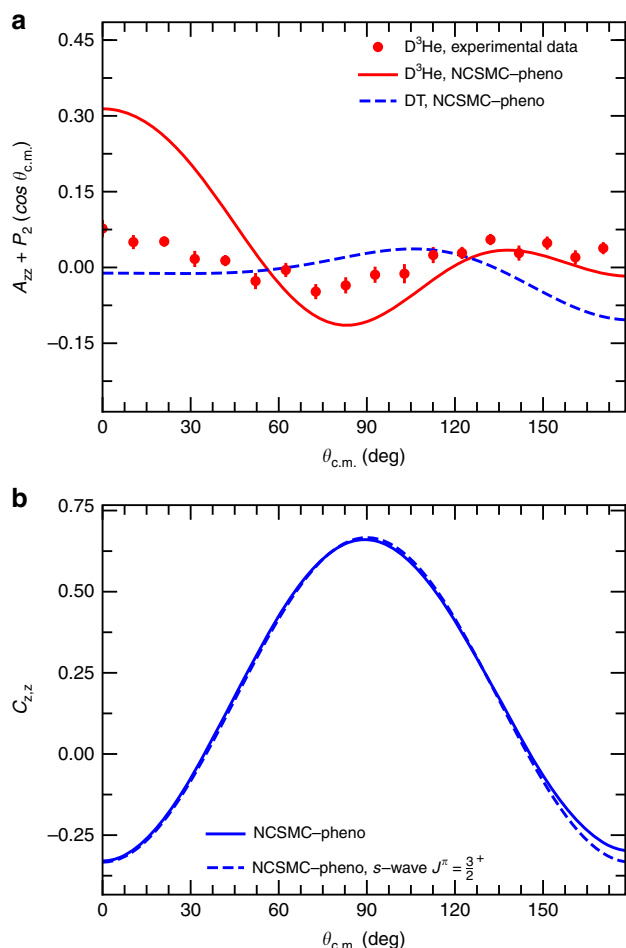


Fig. 3 DT and $D^3\text{He}$ polarization observables. **a** Computed and measured³² tensor analyzing power ($A_{zz}^{(b)}$) of the $D^3\text{He}$ fusion reaction as a function of the scattering angle in the center-of-mass (c.m.) frame, $\theta_{\text{c.m.}}$, at the deuteron incident energy of $E_D = 424$ keV compared to the results for the DT fusion reaction at $E_D = 100$ keV (the corresponding energy, once the difference in the Q -values of the two reactions is taken into consideration). The s -wave contribution to the tensor analyzing power, given by the Legendre polynomial $-P_2(\cos \theta_{\text{c.m.}})$, has been subtracted. The “NCSMC-pheno” label stands for the results of the present calculations after a phenomenological correction of -5 keV to the position of the $3/2^+$ resonance. **b** Computed spin correlation coefficient ($C_{z,z}$) for the DT fusion at $E_D = 128$ keV. The results obtained by disregarding the contribution of partial waves beyond the $J^\pi = 3/2^+$, $\ell = 0$, labeled as “NCSMC-pheno, s -wave $J^\pi = 3/2^+$ ”, are also shown for comparison

are aligned along the z -axis. In practice, however, only the tensor analyzing power at $\theta_{\text{c.m.}} = 0^\circ$ has been measured in the energy region relevant for thermonuclear fusion ($0.24_{-0.18}^{+0.9}$ MeV)³¹. Our computed result (-0.975) agrees well with experiment (-0.929 ± 0.014) (see also Supplementary Note 3 and Supplementary Figs. 6–7). The only available experimental data to test the angular distribution of the differential cross section, and hence the contribution of partial waves other than the $J^\pi = 3/2^+$, $\ell = 0$ component at the relevant energies are measurements of the mirror $D^3\text{He}$ fusion process. Such contribution of additional partial waves is exemplified in Fig. 3a, where we compare theoretical and experimental results for the $D^3\text{He}$ tensor analyzing power at the deuteron incident energy of 0.424 MeV after subtraction of the s -wave contribution, which is simply given by the Legendre polynomial $-P_2(\cos \theta_{\text{c.m.}})$. Our results are in fair agreement with the experimental data³², particularly for what

concerns the shape of the distribution. At the same time, we find notable differences with respect to the predicted DT $A_{zz}^{(b)}$ at the corresponding energy of $E_D = 0.1$ MeV (where we take into account the difference in Q -values), highlighting a somewhat different partial-wave content in the two mirror reactions. This indicates that some caution has to be taken when using $D^3\text{He}$ as a proxy for the study of polarization in the DT fusion process. All in all, Fig. 3a gives added confidence in the polarization observables predicted for the DT fusion. More details on the calculation of the $D^3\text{He}$ reaction observables can be found in Supplementary Note 4 (see also Supplementary Figs. 8–11).

Reaction cross section enhancement. The differential cross section for all angles is required for the computation of the polarized reaction cross section σ_{pol} and the enhancement factor δ , which we obtain (for any initial spin configuration) as the ratio of the latter to σ_{unpol} . As shown in Fig. 4a, at the deuteron incident energy of 100 keV the ab initio calculation recovers and confirms the ideal enhancement factor for $p_z, q_z = 1.0$, which is a result independent of the model space size and the phenomenological correction. Indeed, while our ab initio calculations show that the reaction is not exactly isotropic, at this energy the deviations of $A_{zz}^{(b)}$ and $C_{z,z}$ from a pure $J^\pi = 3/2^+$, $\ell = 0$ contribution are substantial only in the proximity of $\theta_{\text{c.m.}} = 180^\circ$ (see, for example, Fig. 3b), and hence have only a minor effect on angle-averaged observables, such as the reaction cross section. We note that δ is nearly independent of the value of p_{zz} , indicating that the analyzing power of the deuterium does not play any role in the enhancement of the cross section (a consequence of the nearly-zero value of the integral of $A_{zz}^{(b)}$). However, the factor δ varies as a function of the energy and drops significantly above the deuteron incident energy of 0.8 MeV. This is shown in Fig. 4b for the maximum enhancement (which is found for $p_z q_z, p_{zz} = 1$). Interestingly, the peak value of the maximum enhancement (located around $E_D = 0.4$ MeV) is somewhat larger than the estimated 1.5 value. This is mainly an effect of $3/2^+$, $\ell = 2$ contributions. For comparison we also show the maximum enhancement obtained when we only include the $J^\pi = 3/2^+$, and $1/2^+$ partial waves with an orbital relative angular momentum of the $D+T$ pair of $\ell = 0$. This shows the influence of $1/2^+$ components of the wave function below and above the $3/2^+$ resonance even in a purely s -wave picture of the reaction. When also the $1/2^+$ partial wave is removed, we recover the (energy independent) 1.5 estimate.

Reaction rate enhancement. In Fig. 5 we show the polarized fusion reaction rate for typical values of vector and tensor polarization of the deuterium (p_z, p_{zz}) and tritium (q_z) that can be readily obtained in the laboratory, that is $p_z, p_{zz} = 0.8$ and $q_z = 0.8$, respectively. This quantity, obtained from averaging the reaction cross section over the distribution of the reactants’ speeds (assumed to be Maxwellian)³³,

$$\langle \sigma \nu \rangle = \sqrt{\frac{8}{\pi \mu (k_B T)^3}} \int_0^\infty S(E) \exp\left(-\frac{E}{k_B T} - \sqrt{\frac{E}{E_G}}\right) dE,$$

is a measure of how rapidly the reaction occurs and is an important input in astrophysics and plasma simulations. The constant μ is the reduced mass of the reacting nuclei (D and T), k_B and T are respectively the Boltzmann constant and the temperature, $S(E)$ stands for the (computed) S -factor and E_G is the Gamow energy given by $2\mu(\pi e^2)^2/h^2$. In the figure we also compare our unpolarized reaction rate to those obtained from the parameterization of DT fusion data of Bosch and Hale³⁴, the phenomenological R -matrix fit of Descouvemont et al.³⁵, and the potential model calculation adopted in the NACRE

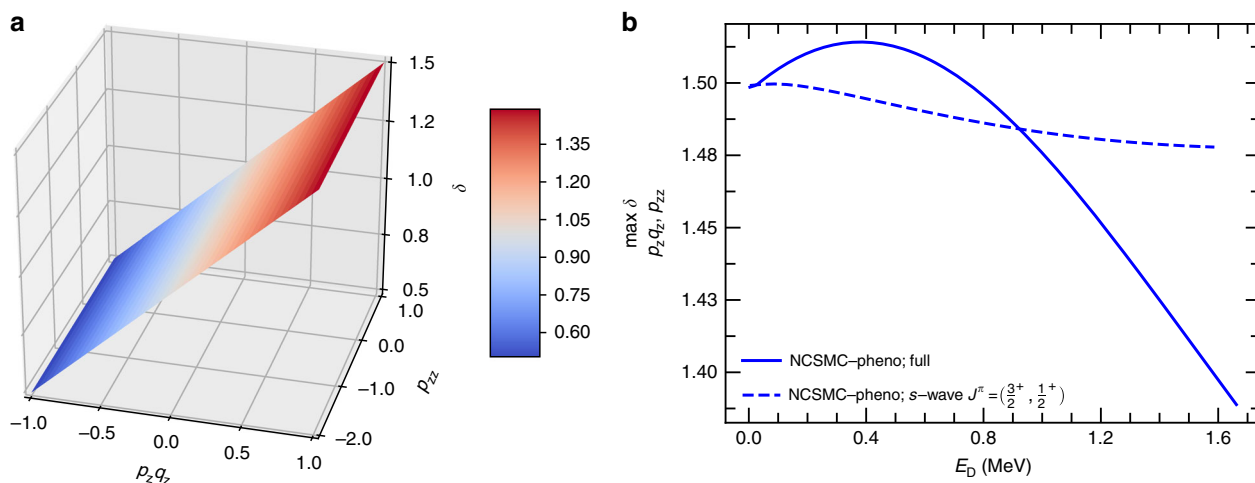


Fig. 4 Enhancement factor of the polarized DT reaction cross section. **a** Present results for the enhancement factor (δ) of the polarized DT reaction cross section at the deuterium incident energy of $E_D = 100$ keV as a function of the vector ($p_z q_z$) and tensor ($p_z z$) polarization of the deuterium and tritium. **b** Computed maximum enhancement factor (over all possible values of $p_z q_z$ and $p_z z$) of the polarized DT cross section as a function of the deuteron incident energy. The maximum enhancement is always found for $p_z q_z, p_z z = 1$. The “NCSMC-pheno; full” label stands for the results of the present calculations including $\ell \neq 0$ partial waves after a phenomenological correction of -5 keV to the position of the $3/2^+$ resonance. Due to the energy scale of the figure, the enhancement factor obtained without such phenomenological correction (that is, the NCSMC result) is indistinguishable from the NCSMC-pheno curve. Also shown is the maximum enhancement factor obtained by retaining only the $\ell = 0, J^\pi = 3/2^+$ and $1/2^+$ partial waves, labeled as “NCSMC-pheno; s-wave $J^\pi = (3/2^+, 1/2^+)$ ”

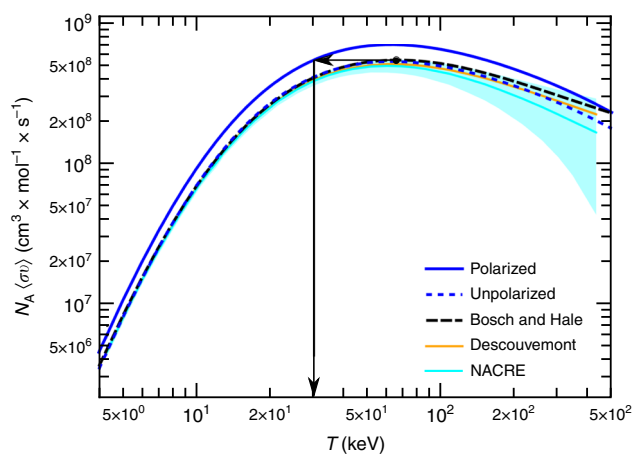


Fig. 5 DT reaction rate with and without polarization. Comparison between the computed DT reaction rate ($N_A \langle \sigma v \rangle$, with N_A the Avogadro number) for unpolarized and polarized fuel with aligned spins as a function of the temperature, T . The “Polarized” and “Unpolarized” labels stand for the present results obtained with the phenomenological correction of -5 keV to the position of the $3/2^+$ resonance (dubbed NCSMC-pheno). We use reactants’ polarization parameters achievable in the laboratory, that is $p_z, p_{zz} = 0.8$ and $q_z = 0.8$. Also shown for comparison are the unpolarized reaction rates obtained from the widely adopted parametrization of the DT fusion cross section of Bosch and Hale³⁴ (labeled as “Bosh and Hale”), from the R -matrix fit of Descouvemont³⁵ (labeled as “Descouvemont”) and from the NACRE compilation³⁶ (labeled as “NACRE”). The arrows in the figure show that, with polarization, a reaction rate of equivalent magnitude as the apex of the unpolarized reaction rate is reached at lower temperatures

compilation³⁶, which is intended for applications in astrophysics simulations. Overall, we find that they agree well even at energies above the resonance. In more detail, our calculation agrees best with the phenomenological R -matrix evaluation, particularly at higher energies where data are typically scarcer. In our case, the uncertainties due to the finiteness of the model space are

indistinguishable from the line width. The convergence of our ab initio model is discussed in Supplementary Note 1 (see also Supplementary Figs. 1-5 and Supplementary Table 2). A further analysis of the systematic and statistical uncertainties associated with the adopted nuclear interaction model, such as those stemming from the order of the chiral expansion or the uncertainty in constraining its parameters, is presently computationally prohibitive (see also Supplementary Discussion). The phenomenological correction induces a global shift towards the reaction threshold, commensurate with that of the resonance centroid. In practice, this fine tuning is tightly constrained by the requirement to match S-factor data in the energy range below the resonant peak. The polarized reaction rate shows the same shape, albeit globally enhanced by a factor of ~ 1.32 , in agreement with the approximate estimate for the chosen polarization. This result follows from the rather slow variation of the enhancement factor of the reaction cross section as a function of the energy in the narrow Gamow window (deuteron incident energies below a few hundred keV) where the product of the Maxwell–Boltzmann distribution with the tunneling probability of the nuclei through their Coulomb barrier is significantly different from zero. It is interesting to note that with polarization a reaction rate of equivalent magnitude as the apex of the unpolarized reaction rate is reached at lower temperatures, that is less than 30 keV compared to 65 keV (where both rates peak), as highlighted in Fig. 5 by the arrows. As a naive illustration, this means that by using polarized DT fuel the output of a standard fusion reactor could either be enhanced by 32% or its operational temperature decreased by as much as 45%. A more comprehensive discussion of the economics of using polarized fuel in the case of inertial confinement fusion can be found in ref. 4.

Angular distribution of the polarized reaction products. While the deviations from a pure $J^\pi = 3/2^+, \ell = 0$ contribution are small and have only a minor effect, particularly on angle-averaged observables such as the reaction cross section or the reaction rate, they play a somewhat larger role on the angular distribution of

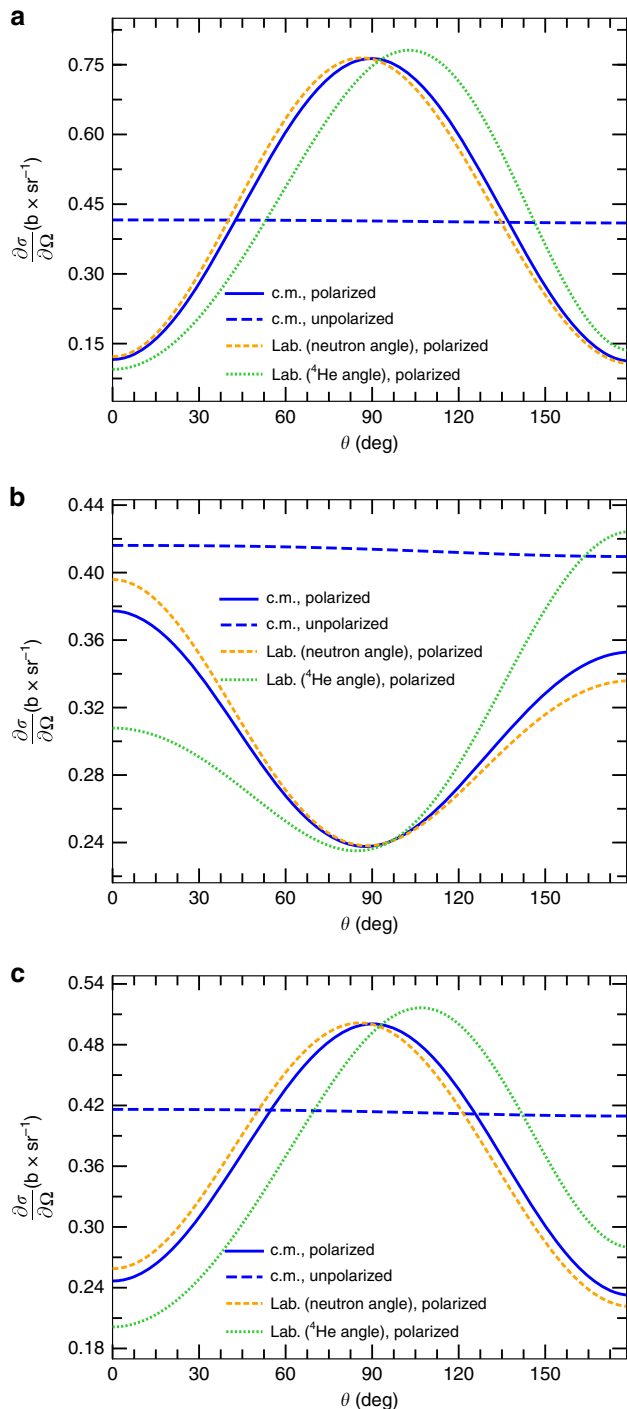


Fig. 6 Present results for the polarized DT differential cross section ($\frac{d\sigma}{d\Omega}$). Three polarization scenarios are shown: **a** With reactants' polarization parameters p_z , $p_{zz} = 0.8$, and $q_z = 0.8$; **b** with spins prepared in an antiparallel setting ($p_z = 0.8$, $q_z = -0.8$ and $p_{zz} = 0.8$); and **c** in the scenario in which only the deuterium is polarized ($p_z = 0.8$ and $p_{zz} = 0.8$). The incident deuterium energy is 100 keV. The "c.m., polarized", "Lab. (neutron angle), polarized", and "Lab. (^4He angle), polarized" labels stand for the polarized differential cross section in the center-of-mass (c.m.) frame, and in the laboratory frame as a function of the neutron and ^4He angles. Correspondingly, θ stands for the c.m., neutron, and ^4He angles. Also shown as a reference is the unpolarized cross section in the c.m. frame (labeled as "c.m., unpolarized"). All results were obtained with the phenomenological correction of -5 keV to the position of the $3/2^+$ resonance (dubbed NCSMC-pheno)

the reaction products, especially when the reactants' spins are not in a parallel setting. In particular, while the tensor analyzing power $A_{zz}^{(b)}$ has virtually no impact on the enhancement factor, it is the main driver of the shape of the angular distribution of the polarized cross section, shown in Fig. 6. To better visualize the situation in the laboratory, in addition to the differential cross section in the c.m. frame we also plot the differential cross section in the laboratory frame as a function of the laboratory neutron and α -particle angles in yellow short-dashed and green dotted lines, respectively. The anisotropy of the angular differential cross section is highly sought after because it can be used to force the emitted neutrons and α to be two to five times more focused towards the reactor blanket (Fig. 6a, c), which collects the energy released, than along the polarization axis, or twice the exact opposite (see Fig. 6b). That is, the reaction products are more focused along the magnetic field. The former conditions can be achieved using only polarized deuterium or fully polarized DT fuel. The latter is obtained in the situation where the D and T spins are anti-aligned, leading to a reduction of the cross section of up to a factor of 0.5, as illustrated in Fig. 4a.

Discussion

In conclusion, we have performed ab initio NCSMC calculations with modern chiral EFT NN and 3N interactions for the DT fusion and its mirror D^3He reaction. We were able to reproduce the cross sections of these reactions with unpolarized reactants. Our calculations discriminate among DT reaction rates from phenomenological evaluations and demonstrate in detail the small contribution of $\ell > 0$ partial waves in the vicinity of the $3/2^+$ resonance. We predict the DT reaction rate for realistically polarized reactants ($p_z, q_z \sim 0.8$) and show that the reaction rate increases by about 32% compared to the unpolarized one and, further, the same reaction rate as the unpolarized one can be achieved at $\sim 45\%$ lower temperature. These results also endorse the application of the present approach to the evaluation of the polarized DD fusion, where the non-resonant character of the reaction prevents even a simple estimate of the enhancement factor in the ideal scenario of perfect spin-alignment of the reactants.

Methods

No-core shell model with continuum. Our approach to the description of the DT fusion reaction is the ab initio NCSMC introduced in ref. 19 and applied to nucleon^{9,11,12}, deuterium³⁷, tritium, and ^3He induced reactions³⁸ and the three-cluster continuum dynamics of the Borromean ^6He nucleus^{39,40}. Presently, it is the only ab initio reaction method capable to efficiently describe complex light-nuclei reactions and in particular transfer reactions, though a complementary approach based on lattice EFT offers a more efficient avenue to the calculation of scattering and reactions induced by α particles⁴¹.

The approach starts from the wave functions of each of the colliding nuclei and of the aggregate system, obtained within the ab initio no-core shell model (NCSM)²⁰ by working in a many-body harmonic oscillator (HO) basis. This is a configuration interaction method in which all nucleons are treated as active degrees of freedom and the model space includes all possible excitations of the system up to a maximum of N_{max} quanta above the minimum-energy configuration. It then uses the NCSM static solutions for the aggregate system and continuous "microscopic-cluster" states, made of pairs of nuclei in relative motion with respect to each other, as an over-complete basis to describe the full dynamical solution of the system. That is, the ansatz for the five-nucleon ($A = 5$) wave function takes the form of a generalized cluster expansion (here specifically shown for the present case of a ^3He aggregate system):

$$|\Psi^{JI}\rangle = \sum_{\lambda} c_{\lambda}^{JI} |^5\text{He}; \lambda J^{\pi} I\rangle + \sum_{\nu} \int dr r^2 \frac{y_{\nu}^{JI}(r)}{r} \hat{A}_{\nu} |\Phi_{\nu}^{JI}\rangle,$$

where J , π and I denote respectively total angular momentum, parity, and isospin quantum numbers. The first term on the right-hand side of the equation is an expansion over the discrete energy eigenstates of the ^5He nucleus (indexed by λ) obtained within the NCSM method to incorporate the physics of the five nucleons in close contact. The second term is tailored to tackle the scattering and long-range clustering of the system. The index $\nu = \{\nu_{\text{TD}}, \nu_{\text{an}}\}$ runs over the reaction channels,

defined by the mass partition (D+T and n+⁴He, respectively) and the quantum numbers characterizing the reacting bodies and their relative motion. The continuum basis states $\Phi_{\nu,r}^{J^{\pi I}}$ are antisymmetrized by the operator \hat{A}_{ν} , and, in the case of the present binary collision, read:

$$|\Phi_{\nu_{TD},r}^{J^{\pi I}}\rangle = \left[[[[{}^3\text{H}; \lambda_T I_T^{\pi T} I_T] ; {}^2\text{H}; \lambda_D I_D^{\pi D} I_D]]^{\text{srT}} Y_{\ell_{TD}}(\hat{r}_{TD}) \right]^{J^{\pi I}} \frac{\delta(r - r_{TD})}{rr_{TD}},$$

and

$$|\Phi_{\nu_{an},r}^{J^{\pi I}}\rangle = \left[[[[{}^4\text{He}; \lambda_{\alpha} I_{\alpha}^{\pi \alpha} I_{\alpha}] |n\rangle]]^{\text{san}} Y_{\ell_{an}}(\hat{r}_{an}) \right]^{J^{\pi I}} \frac{\delta(r - r_{an})}{rr_{an}}.$$

The first set of continuum states describes the incoming T and D nuclei in relative motion, with \hat{r}_{TD} the separation between their centers of mass, while the second set represents the outgoing wave of relative motion between the ejected α and neutron particles with separation \hat{r}_{an} . (Expressions in squared brackets denote angular momentum coupling.) The discrete coefficients $C_{\lambda}^{J^{\pi I}}$ and continuous amplitudes of relative motion $\gamma_{\nu}^{J^{\pi I}}(r)$ are obtained by solving the generalized eigenvalue problem derived from representing the non-relativistic Bloch–Schrödinger equation in the model space spanned by the discrete and continuum basis states of the NCSMC. The scattering matrix—and from it all reaction observable—are finally obtained by matching these solutions with the known asymptotic behavior of the wave function at $r = 18$ fm, using the coupled-channel R -matrix method on a Lagrange mesh^{42,43}.

Details of the calculation. We start from a five-nucleon Hamiltonian including NN⁴⁴ and 3N^{45,46} interactions at the fourth and third order of chiral EFT, respectively, with a 500 MeV cutoff (also adopted in the studies of refs. 9 and 37). This interaction is then softened by the means of the similarity renormalization group (SRG) technique to a resolution scale of $\Lambda_{\text{SRG}} = 1.7 \text{ fm}^{-1}$, enabling good convergence properties within the currently largest HO basis size achievable. The computational challenges of the present work limited such a basis size to a maximum number of HO excitations of $N_{\text{max}} = 11$. For the HO frequency, we chose the value of $\hbar\omega = 16$ MeV, which was found to speed up the convergence rate with respect to N_{max} (see Supplementary Note 1, Supplementary Figs. 4 and Supplementary Table 2).

Besides the size of the HO model space, the convergence properties of the present calculations are also affected by the number of discrete eigenstates of the 2-,3-,4- and 5-nucleon systems used to construct the NCSMC trial wave function. We included the first 14 discrete energy eigenstates of the ⁵He system (two $J^{\pi} = 1/2^{-}$, three $3/2^{-}$, $5/2^{-}$, $7/2^{-}$, three $1/2^{+}$, two $3/2^{+}$, $5/2^{+}$, $7/2^{+}$), the ground state and up to 8 positive-energy eigenstates (5 in the ³S₁-³D₁ and 3 in the ³D₂ channels) of the deuterium, and the ground states of the ³H and ⁴He nuclei. The close vicinity of the energy continuum of the deuterium, only bound by 2.224 MeV, leads to distortion effects the description of which necessitates the inclusion of positive-energy eigenstates^{7,37}. Analogous distortion effects are less pronounced in the more bound triton and α particles, and are efficiently addressed indirectly through the inclusion of the eigenstates of the aggregate ⁵He system^{9,10}.

A particular challenge in the presence of 3N forces is the dependence on the parameter $E_{3\text{max}}$. This embodies the size of the three-nucleon single-particle HO basis used to represent the 3N interaction. For technical reasons, the largest $E_{3\text{max}}$ value computationally achievable is currently of 17 HO quanta. High energy 3N force components of the NCSMC Hamiltonian can be slowly converging as a function of this parameter. Since they represent a small perturbation with respect to the NN contribution, we omit them for basis states at the boundary of the model space.

Phenomenological correction. Remaining inaccuracies in the adopted chiral Hamiltonian prevent an accurate (of the order of less than a few keV) reproduction of the sub p -shell levels. This was already observed for the ⁵He system in, e.g., Figure 16 of ref. 10, which illustrates the residual imprecisions for the reproduction of p -shell spectroscopy. It is then not surprising that the DT fusion S -factor is not perfectly reproduced (see Fig. 1a). To address this difficulty, we treated the eigenvalue of the second $3/2^{+}$ NCSM energy-eigenstate (one of the static basis states that serve as input to represent our solution) as an adjustable parameter and constrained it to the value that yielded the best fit of the experimental S -factor data for energy below the resonance. In practice, this resulted in a shift of -86 keV of the $N_{\text{max}} = 11$ ⁵He $3/2^{+}$ eigenenergy computed within the NCSM, which was initially -8.186 MeV, while the microscopic n+⁴He and D+T cluster potentials and all other characteristics of the scattering matrix continued to be predicted within the *ab initio* method. The amplitude of the correction is less substantial than it appears. In the NCSMC Hamiltonian, the coupling matrix elements between the aggregate system and microscopic-cluster states are given by the NCSM eigenvalues multiplied by the cluster form factor (the overlap between the two type of basis states). As a consequence, the effect of this adjustment is a considerably smaller shift of -5 keV of the resonance centroid E_r extracted from the $3/2^{+}$ eigenphase shifts computed within the NCSMC, shown in Supplementary Table 1. Because the $3/2^{+}$ resonance is close to the D+T threshold, the S -factor is very sensitive to its centroid. Assuming a Breit–Wigner formula for the reaction cross section one can estimate the S -factor to be proportional to $1/E_r^2$, close to threshold and to follow a

$1/E_{\text{cm}}^2$ slope after the resonance. This explains our results, and why our phenomenological adjustment is tightly constrained by reproducing the S -factor close to threshold. We refer to the modified calculation as NCSMC-pheno.

Data availability

The data acquired in this study are available from the corresponding author upon reasonable request.

Received: 8 March 2018 Accepted: 21 November 2018

Published online: 21 January 2019

References

1. ITER Organization. Home page. <https://www.iter.org/> (2018).
2. Lawrence Livermore National Laboratory, National Ignition Facility & Photon Science. <https://lasers.llnl.gov/> (2013).
3. Kulsrud, R. M., Furth, H. P., Valeo, E. J. & Goldhaber, M. Fusion reactor plasmas with polarized nuclei. *Phys. Rev. Lett.* **49**, 1248–1251 (1982).
4. Temporal, M. et al. Ignition conditions for inertial confinement fusion targets with a nuclear spin-polarized DT fuel. *Nucl. Fusion* **52**, 103011 (2012).
5. Paetz gen. Schieck, H. The status of “polarized fusion”. *Eur. Phys. J. A* **44**, 321–354 (2010).
6. Leemann, C. et al. Die ³He(d,p)⁴He Reaktion mit polarisiertem und unpolarisiertem Target und polarisiertem Deutronenstrahl bei E_d = 430 keV. *Helv. Phys. Acta* **44**, 141–159 (1971). *Ann. Phys.* **66**, 810–815 (1971).
7. Navrátil, P. & Quaglioni, S. *Ab initio* many-body calculations of the ³H(d,n)⁴He and ³He(d,p)⁴He fusion reactions. *Phys. Rev. Lett.* **108**, 042503 (2012).
8. Quaglioni, S. & Navrátil, P. *Ab initio* many-body calculations of n-³H, n-⁴He, p-^{3,4}He, and n-¹⁰Be scattering. *Phys. Rev. Lett.* **101**, 092501 (2008).
9. Hupin, G., Quaglioni, S. & Navrátil, P. Predictive theory for elastic scattering and recoil of protons from ⁴He. *Phys. Rev. C* **90**, 061601 (2014).
10. Navrátil, P., Quaglioni, S., Hupin, G., Romero-Redondo, C. & Calci, A. Unified *ab initio* approaches to nuclear structure and reactions. *Phys. Scr.* **91**, 053002 (2016).
11. Langhammer, J. et al. Continuum and three-nucleon force effects on ⁹Be energy levels. *Phys. Rev. C* **91**, 021301 (2015).
12. Calci, A. et al. Can *ab initio* theory explain the phenomenon of parity inversion in ¹¹Be? *Phys. Rev. Lett.* **117**, 242501 (2016).
13. Otsuka, T., Suzuki, T., Holt, J. D., Schwenk, A. & Akaishi, Y. Three-body forces and the limit of oxygen isotopes. *Phys. Rev. Lett.* **105**, 032501 (2010).
14. Cipollone, A., Barbieri, C. & Navrátil, P. Isotopic chains around oxygen from evolved chiral two- and three-nucleon interactions. *Phys. Rev. Lett.* **111**, 062501 (2013).
15. Hagen, G., Hjorth-Jensen, M., Jansen, G. R., Machleidt, R. & Papenbrock, T. Continuum effects and three-nucleon forces in neutron-rich oxygen isotopes. *Phys. Rev. Lett.* **108**, 242501 (2012).
16. Navrátil, P., Gueorguiev, V. G., Vary, J. P., Ormand, W. E. & Nogga, A. Structure of A=10–13 nuclei with two- plus three-nucleon interactions from chiral effective field theory. *Phys. Rev. Lett.* **99**, 042501 (2007).
17. Weinberg, S. Nuclear forces from chiral lagrangians. *Phys. Lett. B* **251**, 288–292 (1990).
18. Epelbaum, E., Hammer, H.-W. & Meißner, U.-G. Modern theory of nuclear forces. *Rev. Mod. Phys.* **81**, 1773–1825 (2009).
19. Baroni, S., Navrátil, P. & Quaglioni, S. *Ab initio* description of the exotic unbound ⁷He nucleus. *Phys. Rev. Lett.* **110**, 022505 (2013).
20. Barrett, B. R., Navrátil, P. & Vary, J. P. *Ab initio* no core shell model. *Prog. Part. Nucl. Phys.* **69**, 131–181 (2013).
21. Liskien, H. & Paulsen, A. *Atom. Data Nucl. Data Tables* **11**, 569–619 (1973).
22. Conner, J. P., Bonner, T. W. & Smith, J. R. A study of the ³H(d,n)⁴He reaction. *Phys. Rev.* **88**, 468–473 (1952).
23. Arnold, W. R., Phillips, J. A., Sawyer, G. A., Stovall, E. J. Jr & Tuck, J. L. Cross sections for the reactions D(d,p)T, D(d,n)³He, T(d,n)⁴He, and ³He(d,p)⁴He below 120 keV. *Phys. Rev.* **93**, 483–497 (1954).
24. Brown, R. E., Jarmie, N. & Hale, G. M. Fusion-energy reaction ³H(d, α)n at low energies. *Phys. Rev. C* **35**, 1999–2004 (1987).
25. Otuka, N. et al. Nuclear Data Sheets **120**, 272–276 (2014).
26. Drogm, M. & Otuka, N. Evaluation of the absolute angle-dependent differential neutron production cross sections by the reactions ³H(p,n)³He, ¹H(t,n)³He, ²H(d,n)³He, ³H(d,n)⁴He, and ²H(t,n)⁴He and of the cross sections of their time-reversed counterparts up to 30 MeV and beyond. INDC(AUS)-0019 (2015).
27. Ohlsen, G. G. Polarization transfer and spin correlation experiments in nuclear physics. *Rep. Progr. Phys.* **35**, 717–801 (1972).
28. Paetz gen. Schieck, H. Nuclear physics with polarized particles. *Lecture Notes in Physics* 842 (Springer, Heidelberg, 2012).

29. Przewoski, B. V. et al. Analyzing powers and spin correlation coefficients for p+d elastic scattering at 135 and 200 MeV. *Phys. Rev. C* **74**, 064003 (2006).
30. Bém, P. et al. Angular anisotropy of the $^3\text{H}(d,\alpha)n$ reaction at deuteron energies below 200 keV. *Few-Body Syst.* **22**, 77–89 (1997).
31. Dries, L. J., Clark, H. W., Detomo, R. Jr., Regner, J. L. & Donoghue, T. R. $A_{zz}(0^\circ)$ for the charge-symmetric $^3\text{He}(^2d,p)^4\text{He}$ and $^3\text{H}(^2d,n)^4\text{He}$ reactions below 6.75 MeV. *Phys. Rev. C* **21**, 475–482 (1980).
32. Geist, W. H. et al. The $^3\text{He}(^2d,p)^4\text{He}$ reaction at low energies. *Phys. Rev. C* **60**, 054003 (1999).
33. Thompson, I. J. & Nunes, F. M. *Nuclear Reactions for Astrophysics*. (Cambridge University Press, 2009).
34. Bosch, H.-S. & Hale, G. M. Improved formulas for fusion cross-sections and thermal reactivities. *Nucl. Fusion* **32**, 611–631 (1992).
35. Descouvemont, P., Adahchoura, A., Angulo, C., Coc, A. & Vangioni-Flam, E. Compilation and R-matrix analysis of Big Bang nuclear reaction rates. *Atom. Data Nucl. Data Tables* **88**, 203–236 (2004).
36. Angulo, C. et al. A compilation of charged-particle induced thermonuclear reaction rates. *Nucl. Phys. A* **656**, 3–187 (1999).
37. Hupin, G., Quaglioni, S. & Navrátil, P. Unified description of ^6Li structure and deuterium- ^4He dynamics with chiral two- and three-nucleon forces. *Phys. Rev. Lett.* **114**, 212502 (2015).
38. Dohet-Eraly, J. et al. $^3\text{He}(\alpha,\gamma)^7\text{Be}$ and $^3\text{H}(\alpha,\gamma)^7\text{Li}$ astrophysical S-factors from the no-core shell model with continuum. *Phys. Lett. B* **757**, 430–436 (2016).
39. Romero-Redondo, C., Quaglioni, S., Navrátil, P. & Hupin, G. How many-body correlations and a clustering shape ^6He . *Phys. Rev. Lett.* **117**, 222501 (2016).
40. Quaglioni, S., Romero-Redondo, C., Navrátil, P. & Hupin, G. Three-cluster dynamics within the *ab initio* no-core shell model with continuum: How many-body correlations and a clustering shape ^6He . *Phys. Rev. C* **97**, 034332 (2018).
41. Elhatisari, S. et al. *Ab initio* alpha-alpha scattering. *Nature* **528**, 111–114 (2015).
42. Descouvemont, P. & Baye, D. The R-matrix theory. *Rep. Progr. Phys.* **73**, 036301 (2010).
43. Baye, D. The Lagrange-mesh method. *Phys. Rep.* **565**, 1–107 (2015).
44. Entem, D. R. & Machleidt, R. Accurate charge-dependent nucleon-nucleon potential at fourth order of chiral perturbation theory. *Phys. Rev. C* **68**, 041001 (2003).
45. Navrátil, P. Local three-nucleon interaction from chiral effective field theory. *Few-Body Syst.* **41**, 117–140 (2007).
46. Gazit, D., Quaglioni, S. & Navrátil, P. Three-nucleon low-energy constants from the consistency of interactions and currents in chiral effective field theory. *Phys. Rev. Lett.* **103**, 102502 (2009).

Acknowledgements

Computing support for this work came from the Lawrence Livermore National Laboratory (LLNL) institutional Computing Grand Challenge program. This article was prepared by LLNL under Contract DE-AC52-07NA27344. This material is based upon work supported by the U.S. Department of Energy, Office of Science, Office of Nuclear Physics, under Work Proposals No. SCW1158 and SCW0498, and by the Natural Sciences and Engineering Research Council of Canada (NSERC) Grants No. SAPIN-2016-00033. TRIUMF receives funding via a contribution through the Canadian National Research Council of Canada.

Author contributions

G.H. carried out the calculations in consultation with S.Q. and P.N. All authors discussed the results and contributed to the manuscript at all stages.

Additional information

Supplementary Information accompanies this paper at <https://doi.org/10.1038/s41467-018-08052-6>.

Competing interests: The authors declare no competing interests.

Reprints and permission information is available online at <http://npg.nature.com/reprintsandpermissions/>

Publisher's note: Springer Nature remains neutral with regard to jurisdictional claims in published maps and institutional affiliations.



Open Access This article is licensed under a Creative Commons Attribution 4.0 International License, which permits use, sharing, adaptation, distribution and reproduction in any medium or format, as long as you give appropriate credit to the original author(s) and the source, provide a link to the Creative Commons license, and indicate if changes were made. The images or other third party material in this article are included in the article's Creative Commons license, unless indicated otherwise in a credit line to the material. If material is not included in the article's Creative Commons license and your intended use is not permitted by statutory regulation or exceeds the permitted use, you will need to obtain permission directly from the copyright holder. To view a copy of this license, visit <http://creativecommons.org/licenses/by/4.0/>.

This is a U.S. Government work and not under copyright protection in the US; foreign copyright protection may apply 2019